

^{29}SiO ($v = 0$) and ^{28}SiO ($v = 1$) $J = 2 - 1$ maser emission from Orion IRc2

A. Baudry¹, F. Herpin¹ and R. Lucas²

¹ Observatoire de l'Université de Bordeaux, BP 89, F-33270 Floirac, France

² Institut de Radioastronomie Millimétrique, 300 rue de la Piscine, F-38406 Saint Martin d'Hères, France

submitted 11 December 1997; accepted 31 March 1998

Abstract. We have observed with the IRAM interferometer at two different epochs and simultaneously the two transitions $v = 0, J = 2 \rightarrow 1$ and $v = 1, J = 2 \rightarrow 1$ of ^{29}SiO and ^{28}SiO in Orion IRc2. We have made the first maps of ^{29}SiO $v = 0, J = 2 \rightarrow 1$ emission from Orion. These maps and properties of the ^{29}SiO spectra attest to maser emission. Our ^{28}SiO maps show the stable ring of maser spots observed in previous works. Combining our own data with published works we derive that the relative motion between the two ridges of the ^{28}SiO emission ring is less than about 0.7 AU/yr over a period of 7 years. On the other hand, the weak high velocity maser features observed around 30 km s⁻¹ seem to move with respect to the stable ring of ^{28}SiO main emission. Our relative ^{29}SiO ($v = 0$) and ^{28}SiO ($v = 1$) spot maps show that most ^{29}SiO and ^{28}SiO emission features are closely related but have not the same spatial extent. We conclude that these masers are not excited in the same gas layers in agreement with pumping models which predict that various v state masers peak in different spatial regions. In addition, our maps of $v = 0$ and $v = 1$ emission suggest that local line overlaps due to turbulence and high gas temperature do not play a dominant role in the excitation of ^{28}SiO and ^{29}SiO , although excitation effects resulting from the overlap of Doppler-shifted ro-vibrational lines may still be significant.

Key words: ISM: Orion A; star formation; interferometry; masers: ^{29}SiO , ^{28}SiO

1. Introduction

Since the discovery nearly 25 years ago of the SiO molecule in Orion (Snyder & Buhl 1974), SiO masers have been observed in the envelopes of hundreds of late-type stars, and

in the direction of a few galactic HII regions. Orion remains a unique source of SiO emission because it contains all known SiO isotopic species and because it is the only star-forming region exhibiting a very strong maser in the $v = 1, J = 2 \rightarrow 1$ transition. The strong and compact $v = 1$ SiO maser is associated with the luminous infrared source IRc2 and is closely connected with the extended and weaker $v = 0$ maser emission mapped at 43 GHz (Chandler & De Pree 1995) and 86 GHz (Wright et al. 1995). Recent high resolution observations showed that IRc2 is a complex object resolved into four components (Dougados et al. 1993) and that the center of the strong ($v = 1$) and weak ($v = 0$) SiO maser outflows coincide with the radio continuum source I (Menten & Reid 1995, Wright et al. 1995), and is displaced from the center of the molecular hot core (lying to the east of source I). On the other hand, the center of the large-scale high velocity bipolar outflow traced by CO lies roughly 3" to the north of source I.

Considerable efforts have been made to properly model the SiO maser phenomenon in late-type stars. Models include radiative and/or collisional excitation schemes (e.g. Kwan & Scoville 1974, Elitzur 1980, Langer & Watson 1984, Lockett & Elitzur 1992 or Bujarrabal 1994). All models share two general characteristics: (i) they require high volumic densities of order $10^8 - 10^{10}$ cm⁻³; (ii) inversion of the SiO level populations depends on the column density, and maser emission in higher vibrational states peaks at higher values of the column density. On the other hand, there are major observational facts that cannot be explained by any of the present radiative/collisional SiO pumping schemes. In particular, the "standard" pumping schemes fail to explain in stars the peculiar distribution of line intensities within a given vibrational state (e.g. Cernicharo & Bujarrabal 1993), and fail to explain the absence or weakness of $v = 2, J = 2 \rightarrow 1$ emission from Orion and late-type stars (Olofsson et al. 1981 b, Bujarrabal et al. 1996). In fact, line overlaps among transitions of the isotopic species of silicon monoxide are an im-

portant addition to radiative/collisional pumping in stars (e.g. González-Alfonso & Cernicharo 1997), while the line overlap between two near infrared lines of SiO and water explains the weakness of the $v = 2, J = 2 \rightarrow 1$ transition (Bujarrabal et al. 1996).

Depending on the relative importance of property (ii) above (namely various v state masers should peak in different spatial regions) with respect to line overlap effects among nearby transitions of SiO and isotopes the spatial distribution of various vibrational transitions should differ or not. Therefore, high spatial resolution and sensitive maps of SiO and isotopes should provide a test of these predictions. With this idea in mind we have compared the spatial distributions of two nearby transitions of ^{29}SiO and ^{28}SiO toward Orion IRc2 which contains the strongest SiO source in the sky. In Sect. 2 we present our observations and give details of data reduction. In Sect. 3 we discuss spectral variability and present our maps of ^{29}SiO and ^{28}SiO emission from Orion. In Sect. 4 we discuss some properties of the apparent ring of ^{29}SiO and ^{28}SiO masers, the relative spatial extents of both species and implications on their excitation. Some conclusions are summarized in Sect. 5.

2. Observations and data reduction

In order to compare the relative spatial distributions of the main (^{28}SiO) and rare isotope (^{29}SiO) emissions we need a relative positional accuracy better than the extent of the main isotope emission, $\approx 0.15''$. For this kind of accuracy simultaneous observations of two different transitions are appropriate. We thus searched for nearby frequencies involving rotational levels not too high in energy. The frequencies of the $v = 0, J = 2 \rightarrow 1$ and $v = 1, J = 2 \rightarrow 1$ transitions of ^{29}SiO and ^{28}SiO (85.75913 and 86.24337 GHz) differ by less than the 500 MHz instantaneous bandwidth of the interferometer and can thus be simultaneously observed. Observations of these two lines in Orion IRc2 were made on August 19 and 21, 1995 and March 5, 1996 with four antennas of the IRAM array on Plateau de Bure (see Guilloteau et al. 1992 for details). In 1995 we used configuration B2 with antennas on stations N17 E24 W09 W12 and spacings covering 24 to 288 m. The synthesized beam was around $3.5'' \times 1.4''$. Higher spatial resolution was achieved in 1996 with antennas on stations N29 E24 W20 W27 corresponding to spacings from 56 to 408 m and resulting in $2.6'' \times 1''$ resolution. The independent correlator units of the interferometer were used as follows. The $v = 0, J = 2 \rightarrow 1$ and $v = 1, J = 2 \rightarrow 1$ lines of ^{29}SiO and ^{28}SiO were placed in two 20 MHz sub-bands centered at 113.75 MHz and 596.25 MHz, respectively. The frequency separation between adjacent spectral channels was 78.1 kHz, or 0.27 km s^{-1} . In 1995, for redundancy, the ^{29}SiO $v = 0$ line was also observed in a 40 MHz wide sub-band. Broad band continuum observations with three or two 160 MHz units were performed simultaneously.

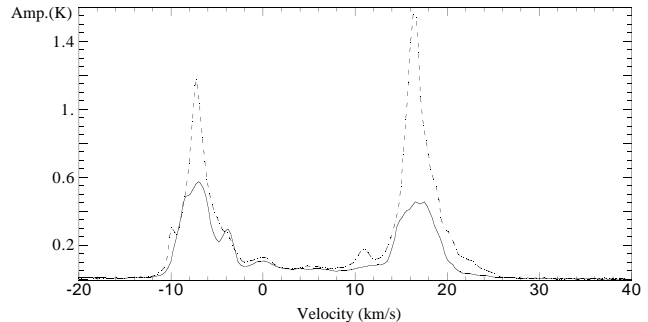


Fig. 1. Cross-correlation spectrum of the $v = 0, J = 2 \rightarrow 1$ line of ^{29}SiO observed with the IRAM array on 1995 August (continuous line) and 1996 March (dotted line). The separation between channels was 0.27 km s^{-1} . 1 K corresponds to a flux density of 24 Jy.

In this project we have mapped the ^{29}SiO and ^{28}SiO line emissions using one of the strongest features of the main isotopic species to self-calibrate all data. Therefore, a careful bandpass calibration was required across the entire bandwidth since the maximum frequency separation between extreme features of both species is around 496 MHz. To this end we observed strong calibrators, 3C454.3, 3C273, 0528 + 134 or 0415 + 379. In 1995 our best results were obtained with 3C454.3 which we observed just before a long run in Orion. Although we do not expect a priori any short time-scale variations of the bandpass shape, we used a different scheme in 1996. Observations of Orion were interspersed with those of the bandpass calibrator 0415 + 379. Nearby phase calibrators were not essential for this project since we self-calibrate the data on one of the main spectral features. The bandpass calibrators were used to calibrate the flux density scale. At 86 GHz we adopted 6.5 and 10 Jy for 3C454.3 (1995 August observations) and 0415 + 379 (1996 March observations), respectively. Although the flux density for 0415 + 379 was uncertain because it was highly time variable in 1995 and 1996, we averaged our measurements of the antenna temperature to Jy conversion factor for both observing periods and adopted $S/T = 24 \text{ Jy/K}$.

Data reduction was performed with the CLIC package (Lucas 1996). The sky was clear during the observations and little editing was necessary. However, we discarded some of the 1995 data when Orion was too low on the horizon. The bandpass solutions were determined by fitting the complex gains in several sub-bands; these solutions were applied to the line data base. In 1995 each day was treated separately. To improve the phase stability we determined accurate baseline solutions and we applied the known antenna axis corrections. The phase residuals lied in the range $4 \rightarrow 30$ and $4 \rightarrow 8$ degrees

Table 1. Signal to noise ratio and errors for observations of 1996 March (the synthesized beam is of order $1.6''$).

SNR and Error	^{28}SiO	^{29}SiO	$^{29}\text{SiO} / ^{28}\text{SiO}$
SNR	200-25000	150-400	150-25000
r.m.s. phase (degree) ¹	0.002-0.29	0.14-0.38	0.14-0.48
r.m.s. position (mas)	0.03-4	2.0-5.3	2.0-6.6
bandpass phase (degree) ²	1	1	
phase shift (degree) ³			1
position shift (mas)			4.4

¹Phase noise due to finite signal to noise ratio; the corresponding position error is $\sigma_\phi \simeq 0.5 \times 1.6'' / \text{SNR}$.

²Typical total bandpass phase noise; the channel to channel IF noise is negligible and less than 0.1 degree.

³Maximum phase shift between ^{28}SiO and ^{29}SiO sub-bands; one degree phase shift corresponds to 4.4 mas with $1.6''$ synthesized beam.

for the 1995 and 1996 observations, respectively. We then mapped the ^{28}SiO and ^{29}SiO line emissions using the task UV_ASCAL and one strong feature of the main isotope to self-calibrate all other features. Accordingly, we are insensitive to atmospheric phase fluctuations and to any systematic errors left in the baseline calibration. The position accuracy within the ^{28}SiO and ^{29}SiO spot maps is limited by finite signal to noise ratio and by imperfect bandpass calibration (see Table 1). In practice, the position errors within our ^{28}SiO maps lie around $1 - 2$ milliarc sec (mas) in RA and $4 - 5$ mas in Declination. This allows us to discuss the long-term stability of the velocity pattern observed for both isotopes, as well as the long-term stability of the ^{28}SiO emission ring discussed in Sect. 4.1. When one compares the relative positions of the ^{29}SiO and ^{28}SiO emissions, the relative phase shift of the two ^{28}SiO and ^{29}SiO sub-bands cannot be neglected (Table 1); we found a maximum drift of 1 degree per hour for the March 1996 observations. Because we regularly calibrated the bandpass in 1996, the position error between both isotopic species due to phase shift between sub-bands was less than 5 mas. This error is estimated to be about ten times higher in our data of 1995 August due to much less time spent in bandpass calibration. In Sect. 4.4, we only discuss the relative positions of both isotopic species observed in 1996. The overall relative ^{28}SiO to ^{29}SiO position uncertainty is of order 5-8 mas.

3. Results

3.1. $^{29}\text{SiO } v = 0, J = 2 \rightarrow 1$ emission

The $^{29}\text{SiO } v=0$ line at 85.759 GHz was discovered in Orion by Olofsson et al. (1981 a) who observed narrow and time variable features. The maser nature of this emission is well demonstrated here because we detect narrow spectral emission of same intensity with all baselines of the array. $^{29}\text{SiO } v = 0$ emission will be discussed further in Sect. 4.2 and is essentially unresolved with the IRAM connected ar-

ray (see below, however). In addition, we observe spectral variability over the 6.5 months period of our two observing sessions since both the line shape and relative peak intensities clearly changed with time (Fig. 1). The emission spectrum consists of two main features in the velocity range $-11 \rightarrow 0$ and $10 \rightarrow 24 \text{ km s}^{-1}$. This is similar to the ^{28}SiO emission range although ^{29}SiO and ^{28}SiO emission profiles are much different, a fact which can partly be related to differences in the degree of saturation of both masers. There is weak emission in the intermediate velocity range $0 \rightarrow 10 \text{ km s}^{-1}$. This ^{29}SiO emission is about 20 times weaker than in ^{28}SiO , and is detected with all baselines of the array. However, with the 24-m long baseline available in 1995, the ^{29}SiO emission lying between the two main features was nearly 5 times stronger than for all other longer baselines. We conclude that for this baseline there was a blend of quasi-thermal and maser ^{29}SiO emission. Both maser emission and quasi-thermal emission were also observed in the $v = 0$ state of the more abundant species ^{28}SiO (Chandler & De Pree 1995, and Wright et al. 1995 for the $J = 1 - 0$ and $J = 2 - 1$ transitions, respectively). Wright et al. showed that the $^{28}\text{SiO } v = 0$ maser component extends over $\approx 2''$ although it is closely connected with the $v = 1, J = 2 - 1$ compact masers. On the other hand, their $^{28}\text{SiO } v = 0$ low spatial resolution maps are more sensitive to thermal emission and show a connection with the high velocity bipolar CO outflow ($\approx 25'' \times 45''$ in size). For all ^{29}SiO spectra and data discussed in this work we restricted the analysis to (u, v) distances greater than about 50 m and 25 m for our observations of 1996 March and 1995 August, respectively. We were thus insensitive to structures extending over $\approx 10'' - 30''$.

Fig. 2 shows the relative positions of $^{29}\text{SiO } v = 0, J = 2 \rightarrow 1$ maser spots observed in 1996. We used the strong $^{28}\text{SiO } v = 1, J = 2 \rightarrow 1$ maser feature at 15.6 km s^{-1} to self-calibrate these data (cf. Sect. 2), and we verified that selection of a specific reference feature was not critical. The $^{29}\text{SiO } v = 0$ emission is distributed along two ridges of positive and negative velocities as for ^{28}SiO (compare Fig. 2 with Figs. 4 and 5) with stronger $^{29}\text{SiO } v = 0$ features excited at the edge of each ridge contrary to ^{28}SiO . The mean distance between the two ^{29}SiO ridges is of order $0.13'' - 0.14''$. This picture is fully consistent with our 1995 results although the mean distance between the two ridges was slightly narrower in 1995 and of order $0.11''$. The 20 to 30 mas change between the two ridges observed in 1995 and 1996 seems real because it is greater than the typical relative position error of the individual ^{29}SiO features. At both epochs of observations the data were acquired with non rotating antenna feeds sensitive to vertical polarization only. However, we are not affected by polarization effects because we have verified that our relative spot maps were nearly identical when we analyzed the data over short periods with a small range of parallactic angle.

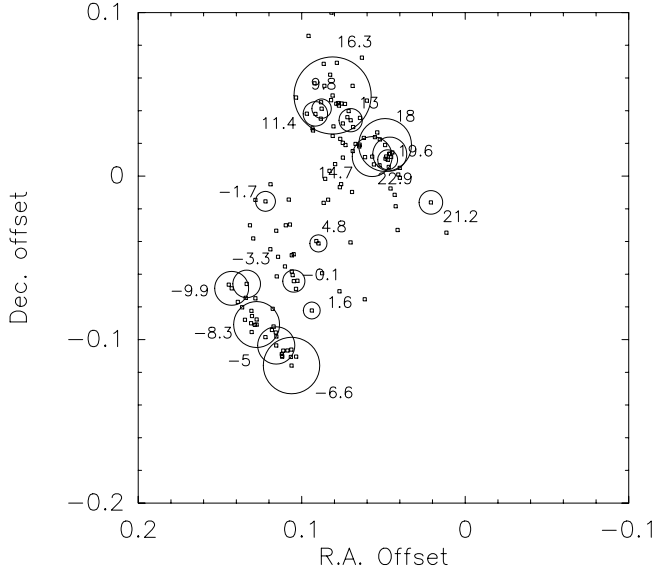


Fig. 2. Spot map of $^{29}\text{SiO } v = 0, J = 2 \rightarrow 1$ emission observed on 1996 March. The small open squares correspond to the centroid of emission in one spectral channel. Each channel is separated by 0.27 km s^{-1} . The center of the brighter channels is surrounded by a circle whose diameter is proportional to the peak intensity in these channels. The LSR velocities are shown for the brighter channels, and, for clarity, the circles and velocity labels are given every 6 channels.

3.2. $^{28}\text{SiO } v = 1, J = 2 \rightarrow 1$ emission

The $^{28}\text{SiO } v = 1, J = 2 \rightarrow 1$ spectrum is dominated by two strong, time variable features lying around $-2 \rightarrow -10$ and $12 \rightarrow 20 \text{ km s}^{-1}$. In addition, the line profile exhibits weak features around 30 km s^{-1} which were first detected by Wright et al. (1995; see their Fig. 1). These features are present in our 1995 and 1996 data (Fig. 3). Comparison with the line profile obtained by Wright et al. with similar spectral resolution shows that they are time variable. The peak flux around 30 km s^{-1} is around 18 Jy in Wright et al. while we measured 10 Jy in March 1996. Variability and detectability with all six baselines of the array suggest that these weak features are masing as the bulk of the ^{28}SiO emission; see, however, discussion in Sect. 4.2. Our map of relative positions of $v = 1, J = 2 \rightarrow 1$ maser emission observed in 1995 August is shown in Fig. 4; in Fig. 5 we also show the relative intensities of the main features. The position-velocity pattern present in Fig. 4 or 5 is consistent with our 1996 observations (open squares and small full circles in Fig. 6) and with that observed in 1995 January by Wright et al. (1995). All maps show similarities. There are, however, minor but obvious changes among the different maps including changes for the weak high velocity features which seem to have moved during the period 1995 January to 1995 August and 1996 March.

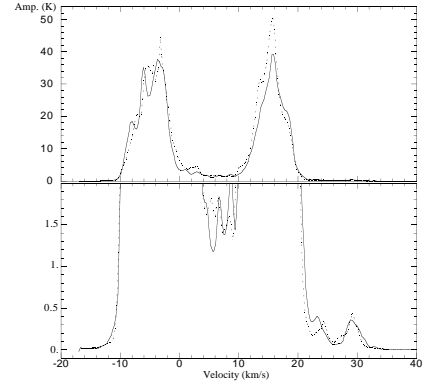


Fig. 3. Cross-correlation spectrum of $^{28}\text{SiO } v = 1, J = 2 \rightarrow 1$ emission observed on 1995 August (continuous line) and 1996 March (dotted line). The upper panel shows the overall spectrum and the lower panel shows the weak features around 23 to 33 km s^{-1} and intermediate velocity emission around $4 \rightarrow 10 \text{ km s}^{-1}$. The separation between individual channels is 0.27 km s^{-1} . 1 K corresponds to a flux density of 24 Jy.

On the other hand, the mean distance between the main negative and positive velocity features remains stable. For our 1996 observations we measured a separation of $0.16''$, a value very close to that deduced from our 1995 results and earlier IRAM results, and consistent with the BIMA array results (see discussion in Sect. 4.1). The absolute position of the ^{28}SiO maser was measured by Wright et al. (1990) and Baudry et al. (1995) to an accuracy of $\approx 0.15'' - 0.20''$. Menten & Reid (1995) found that the centroid of the SiO maser distribution coincides with the radio continuum source, I, lying on the southern edge of the complex source IRc2.

4. Discussion

4.1. Stability of the ring of ^{28}SiO masers

The regular position-velocity pattern of $v = 1, J = 2 \rightarrow 1$ emission (Plambeck et al. 1990, Wright et al. 1995) was interpreted by Plambeck et al. as a collection of maser clumps lying in an expanding and rotating disk. This pattern does not change much with time and has been observed with the IRAM interferometer in 1990 (Guilloteau et al. 1992), 1992 (Baudry et al. 1995), and 1995 and 1996 (this work). A similar position-velocity pattern was also observed in the $J = 1 \rightarrow 0$ transition of SiO around 43 GHz by Morita et al. (1992) and Menten & Reid (1995). We

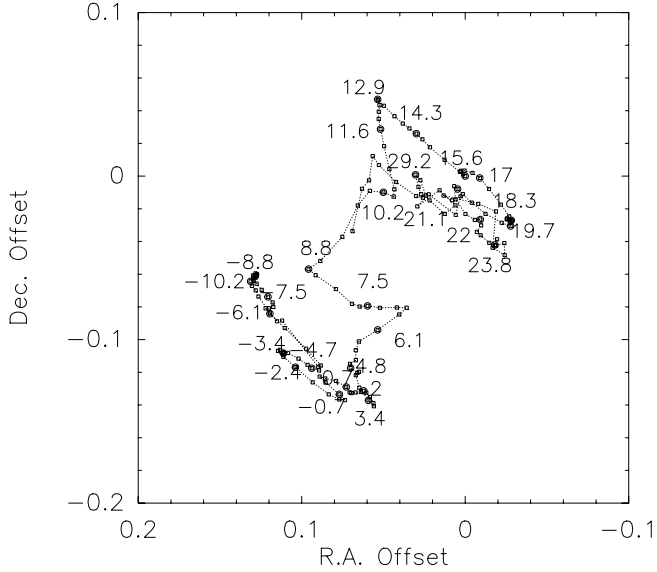


Fig. 4. Spot map of $^{28}\text{SiO } v=1, J=2 \rightarrow 1$ emission observed on August 19, 1995. Each velocity channel is connected and, for clarity, the LSR velocity labels are given every 5 channels. The velocity separation between each open square is 0.27 km s^{-1} .

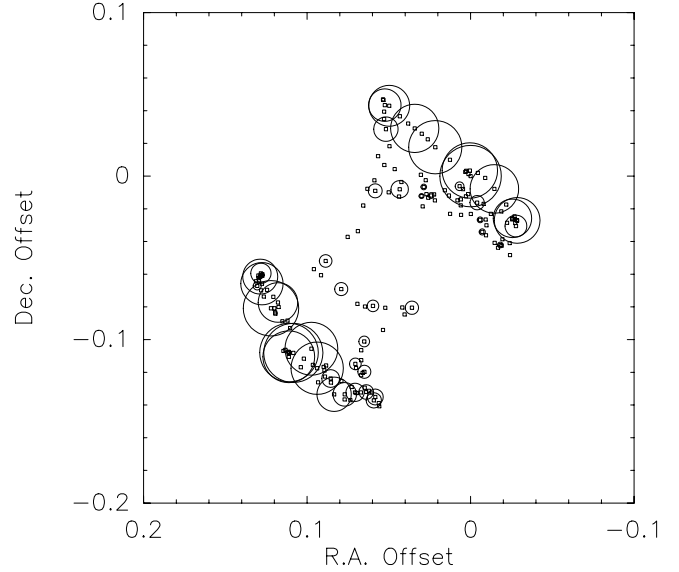


Fig. 5. Spot map of $^{28}\text{SiO } v=1, J=2 \rightarrow 1$ emission observed on August 19, 1995. Each small open square marks the center of an individual channel whose velocity is given in Figure 4. The diameter of each circle, given every 3 channels, is proportional to the line intensity.

can estimate the long-term stability of the 86 GHz pattern by measuring the mean separation between the two ridges delineated by the dominant positive and negative velocity features of Orion IRc2. To this end, we have used the 6 different maps made at 86 GHz with the BIMA and IRAM interferometers (Plambeck et al. 1990, Wright et al. 1995, Guilloteau et al. 1992, Baudry et al. 1995, and this work). The general orientation and the mean separation between the two ridges of main SiO features do not seem to evolve with time. The mean separation between these two ridges is $\approx 0.''165 \pm 0.''01$; for the uncertainty we have assumed that the 6 independent measurements behaved as gaussian variables. Therefore, any apparent contraction or expansion of the ring, would be less than or of order $0.''01/7\text{yr}$, namely $\leq 0.7 \text{ AU/yr}$ at the 480 pc distance of Orion A. On the other hand, stability of the intermediate velocity pattern ($\approx 0 \rightarrow 11 \text{ km s}^{-1}$) is not obvious when we compare our 1990 data with the present IRAM maps. The complex shape observed in 1995 or 1996 is not quite similar to that in 1990 (see Fig. 11 in Guilloteau et al. 1992). Such differences cannot be due to relative position errors which are less than about 2 to 5 mas in the ^{28}SiO maps. These discrepancies seem to agree with the model of Plambeck et al. (1990) which predicts that intensity changes in the intermediate velocity features could cause large position changes of the maser spots in the disk.

4.2. Nature of the ^{28}SiO high velocity features

The high velocity features lying around $28 \rightarrow 31 \text{ km s}^{-1}$ are located close to the positive velocities of the SiO ring (see e.g. the 29.2 and 29.1 km s^{-1} features in Figs. 4 and 6). Our observations of 1995 August show that these features are excited in an area similar, although not identical, to that observed in 1995 January by Wright et al. (1995, see their Fig. 1c) for their $30 \rightarrow 33 \text{ km s}^{-1}$ features. However, 6.5 months later our data show that the $28 \rightarrow 31 \text{ km s}^{-1}$ features have migrated toward the most positive velocity end of the main SiO emission ridge (see location of the 29.1 km s^{-1} component in Fig. 6). The apparent migration of weak high velocity components is consistent with the model of Plambeck et al. (1990) where small changes in brightness distribution of extended features may look like rapid motion. Nevertheless, such rapid motions should be confirmed in future maps of ^{28}SiO emission. These high velocity features could be related to the spectral changes observed for the same components; they could be weakly masing as suggested in Sect. 3.2. It is interesting to note that anomalous gas motion beyond the expansion velocity of the ring of maser clumps could perhaps explain the high velocity components. Such components are reminiscent of the weak features observed in the line wings of ^{28}SiO emission from late type stars (Cernicharo et al. 1997, Herpin et al. 1998). SiO line wing emission in stars

thermal and masing features as suggested in the previous Section.

Fig. 6 shows that velocities in the range $\approx -6 \rightarrow -10$ km s $^{-1}$ tend to be found in the same area for both species although it is not possible to make an exact position-velocity pairing of the ^{29}SiO and ^{28}SiO features. In Fig. 7 the northern ridges of both ^{29}SiO and ^{28}SiO seem to be co-aligned and are not coincident. We cannot exclude, however, that uncorrected instrumental effects still affect our relative map and these observations should be repeated using frequent bandpass calibrations as used in 1996. In order to force the spatial coincidence of the main features in both species we have shifted the main ^{29}SiO features lying around 16 km s $^{-1}$ on top of the ^{28}SiO features in the range $15 \rightarrow 17$ km s $^{-1}$. Nevertheless, the ^{29}SiO negative velocity emission ridge appears well outside the ^{28}SiO negative velocity ridge. Any rotation of coordinates axis around the 16 km s $^{-1}$ features does not improve the spatial coincidence of both species. Hence, we conclude that both isotopic species are not excited in the same gas layers. This is strengthened by the analysis of our 1995 data which similarly show no spatial coincidence and a smaller distance between the two ridges of emission for ^{29}SiO than for ^{28}SiO .

We note that a similar picture also emerges from the 43 GHz interferometric observations made by Morita et al. (1992) in Orion. Although their observations of the ^{28}SiO $v = 2, J = 1 \rightarrow 0$ and $v = 1, J = 1 \rightarrow 0$ transitions were not made simultaneously and were less sensitive than here, the mean separation between the two ridges of emission is slightly smaller for $v = 2$ ($\approx 0.12''$) than for $v = 1$ ($\approx 0.14''$ in agreement with the separation measured on the 43 GHz map of Menten & Reid 1995). The 43 GHz observations, the maps of ^{28}SiO $v = 1$ and $v = 0$ emission (Wright et al. 1995) and our 86 GHz maps indicate that different vibrational states of silicon monoxide do show a close connection but do not exactly coincide.

We comment below on possible explanations of the observed similarities without exact co-location of ^{29}SiO ($v = 0$) and ^{28}SiO ($v = 1$) maser sources. First, the silicon monoxide reservoir seems identical for both isotopic species since their large-scale spatial distributions are alike. This is expected if shocks generated in the expanding flow traced by the $v = 1, J = 2 \rightarrow 1$ masers enhance the sputtering of silicon which will then react quickly in the gas phase to form both ^{29}SiO and ^{28}SiO . Second, differences in the small-scale spatial distributions of ^{29}SiO and ^{28}SiO could simply result from differences in the excitation of both species or from different physical conditions within the silicon monoxide cloud. SiO pumping models do not require any isotopic differentiation to obtain ^{28}SiO , ^{29}SiO or ^{30}SiO maser sources. In all cases the general physical conditions are grossly similar for one isotopic species or another apart from the total column densities. On the other hand, all radiative/collisional pumping models show that different v state masers peak

in different spatial regions. We believe that this fact, combined with different degrees of saturation in the ^{28}SiO and ^{29}SiO masers, is essential to explain the slightly different distribution of ^{29}SiO ($v = 0$) and ^{28}SiO ($v = 1$) maser spots. Our maps of relative ^{28}SiO and ^{29}SiO emission also show that some features from both isotopes and with different velocities tend to be excited in the same area. This is observed in the range $-6 \rightarrow -10$ km s $^{-1}$. Collisional pumping with high temperature (≈ 1500 K) and high molecular hydrogen density ($\approx 10^9 - 10^{10}$ cm $^{-3}$) provides a range of ^{28}SiO column densities where both $v = 1$ and $v = 2, J = 1 \rightarrow 0$ masers are excited (Lockett & Elitzur 1992). Such a scheme does not apply to our apparently overlapping ^{29}SiO ($v = 0$) and ^{28}SiO ($v = 1$) 86 GHz features because their velocities are not in good agreement. However, further observations should be conducted to investigate the detailed kinematics and stability of the ^{29}SiO emission.

Line overlap effects among various transitions of silicon monoxide cannot be ignored to explain the excitation of this molecule. First, *local* line overlaps due to turbulence play a role as soon as the velocity dispersion reaches about 5 km s $^{-1}$. Limiting ourselves to the lower J values, we find that 10 to 15 ro-vibrational transitions of ^{28}SiO , ^{29}SiO and ^{30}SiO overlap within 5 km s $^{-1}$ for $\Delta v = 2$ and 1. If local line overlaps would dominate the excitation of low J rotational levels in Orion, we would expect exact spatial coincidence of the isotopic species. Our ^{29}SiO and ^{28}SiO maps contradict this idea. Second, *non-local* line overlap effects as described by González-Alfonso & Cernicharo (1997) in a non static circumstellar environment are most important. The relative distribution of ^{28}SiO and ^{29}SiO emission in our maps is not inconsistent with such non-local line overlaps. In addition, it is also plausible that the overlap between two near infrared lines of water and ^{28}SiO (Olofsson et al. 1981 b) is an important excitation process of silicon monoxide in Orion.

Analysing the spatial extents of different v state masers is clearly important to better understand the pumping mechanisms of the SiO molecule. This kind of work should be extended to strong stellar SiO-emitters since the physical conditions in late-type stars and Orion are so different. VLBI observations are required in stars in order to make a detailed comparison of the different v emission layers; such observations have been made for the first time to map the $v = 2, v = 1, J = 1 \rightarrow 0$ lines in W Hya and VY CMa (Miyoshi et al. 1994).

5. Summary

We have made the first spot map of ^{29}SiO $v = 0, J = 2 \rightarrow 1$ emission from Orion, and we confirm its maser nature. However, there is also a blend of thermal emission with maser emission. The ^{29}SiO $v = 0, J = 2 \rightarrow 1$ stronger emission is distributed along two ridges of positive and negative velocities as for the ^{28}SiO $v = 1, J = 2 \rightarrow 1$ tran-

sition. The spatial extent is similar but not identical for the $v = 0$ and $v = 1$ masers in agreement with model calculations which predict that various v state masers peak in different spatial regions. For those apparently overlapping $v = 0$ and 1 features the differences observed in the velocities suggest also that ^{29}SiO and ^{28}SiO lie in different $v = 0$ and 1 gas layers. Turbulence and high gas temperature implying local line overlap effects among transitions of ^{29}SiO and ^{28}SiO are unlikely to play a major role in Orion. However, overlaps among Doppler-shifted ro-vibrational lines are not excluded.

We have discussed the long-term stability of the $^{28}\text{SiO } v = 1, J = 2 \rightarrow 1$ emission disk; relative motion between the two ridges of main emission is less than ≈ 0.7 AU/yr. We confirm the detection of features at velocities as high as about 30 km s^{-1} ; they could be either rapidly moving weak masers or extended features with changing brightness distribution.

Acknowledgements. This work was supported by the CNRS URA 352. We thank the IRAM staff on Plateau de Bure for their efficient help during the observations, and we thank M.C.H. Wright for his useful comments.

References

- Baudry A., Lucas R., Guilloteau S. 1995, A&A 293, 594
 Bujarrabal V. 1994, A&A 285, 953
 Bujarrabal V., Alcolea J., Sanchez-Contreras C., Colomer F. 1996, A&A 314, 883
 Cernicharo J., Bujarrabal V. 1993, ApJ 407, L33
 Cernicharo J., Alcolea J., Baudry A., González-Alfonso E. 1997, A&A 319, 607
 Chandler C.J., De Pree C.G. 1995, ApJ 242, 211
 Dougados C., Léna P., Ridgway S.T. et al. 1993, ApJ 406, 112
 Elitzur M. 1980, ApJ 240, 553
 González-Alfonso E., Cernicharo J. 1997, A&A 322, 938
 Guilloteau S., Delannoy J., Downes D. et al. 1992, A&A 262, 624
 Herpin F., Baudry A., Alcolea J. et al. 1998, A&A in press
 Kwan J., Scoville N. 1974, ApJ 194 L197
 Langer S.H., Watson W.D. 1984, ApJ 284, 751
 Lucas R. 1996, CLIC version 4.1, IRAM internal memo
 Lockett P., Elitzur M. 1992, ApJ 399, 704
 Menten K.M., Reid M.J. 1995, ApJ 445, L160
 Miyoshi M., Matsumoto K., Kameno S. et al. 1994, Nat. 371, 395
 Morita K.I., Hasegawa T., Ukita N. et al. 1992, PASJ 44, 373
 Olofsson H., Hjalmarson A., Rydbeck O.E.H. 1981 a, A&A 100, L30
 Olofsson H., Rydbeck O.E.H., Lane A.P., Predmore C.R. 1981 b, ApJ 247, L81
 Plambeck R.L., Wright M.C.H., Carlstrom J.E. 1990, ApJ 348, L65
 Snyder L.E., Buhl D. 1974, ApJ 189, L31
 Wright M.C.H., Carlstrom J.E., Plambeck R.L., Welch W.J. 1990, AJ 99, 1299
 Wright M.C.H., Plambeck R.L., Mundy L.G., Looney L.W. 1995, ApJ 455, L185

This article was processed by the author using Springer-Verlag L^AT_EX A&A style file L-AA version 3.